High-Energy Diffraction Microscopy at the Advanced Photon Source

U. Lienert, S.F. Li, C.M. Hefferan, J. Lind, R.M. Suter, J.V. Bernier, N.R. Barton, M.C. Brandes, M.J. Mills, M.P. Miller, B. Jakobsen, and W. Pantleon

The status of the High Energy Diffraction Microscopy (HEDM) program at the 1-ID beam line of the Advanced Photon Source is reported. HEDM applies high energy synchrotron radiation for the grain and sub-grain scale structural and mechanical characterization of polycrystalline bulk materials in situ during thermomechanical loading. Case studies demonstrate the mapping of grain boundary topology, the evaluation of stress tensors of individual grains during tensile deformation and comparison to a finite element modeling simulation, and the characterization of evolving dislocation structure. Complementary information is obtained by post mortem electron microscopy on the same sample volume previously investigated by HEDM.

INTRODUCTION

High-energy x-rays (50–100 keV) penetrate millimeters to centimeters into materials, depending on the atomic numbers of the constituents, and therefore are capable of probing true bulk properties. High-energy third generation synchrotron facilities such as the Advanced Photon Source (APS) at the Argonne National Laboratory provide high-energy x-rays of unprecedented brilliance enabling the preparation of intense sub-micrometer sized beams. It has been demonstrated that by using area detectors and exploiting orientation contrast, diffraction of such beams by polycrystalline materials enables characterization of structural attributes and grain-scale mechanical properties and performance characteristics in situ during thermomechanical loading.[1] Over the last several years specialized instrumentation has been developed at the APS 1-ID beamline within the High-Energy Diffraction Microscopy (HEDM) project which has grown to be a major user program. This paper outlines distinct HEDM techniques and presents case studies. Details of x-ray optical components may be found elsewhere.[2]

How would you…

…describe the overall significance of this paper?

This paper describes emerging characterization experiments referred to as High Energy Diffraction Microscopy conducted at the Advanced Photon Source (APS) beam line 1-ID-C. "Near field" diffraction is used to quantify three-dimensional orientation maps of polycrystalline samples non-destructively, with incredible detail grain boundary geometry. "Far field" experiments are used to quantify lattice strains and single crystal stress states within large aggregates subjected to in situ loading.

…describe this work to a materials science and engineering professional with no experience in your technical specialty?

Materials derive their mechanical properties from their internal structure. As engineering moves downscale, it becomes more important to quantify the structure and mechanical response of engineering materials on small size scales. High energy x-ray diffraction methods are rapidly evolving into important microscale characterization tools that can be used together with high fidelity mechanical models.

…describe this work to a layperson?

Micro- and nano-engineering methods hold enormous promise for a broad spectrum of products and processes. The determination of material attributes and mechanical properties on small size scales is one of the main barriers to moving down scale. Instead of making tiny specimens, we examine deforming test samples using high energy x-rays, created using a special national laboratory facility. This work will enable us to precisely reconstruct the internal structure of engineering alloys and will provide important mechanical data on the micron scale.

Types of diffraction experiments on polycrystals can be generally delineated in terms of the sample-to-detector distance. In the near-field limit, grain outlines are projected onto a high-resolution imaging detector which is placed only a few millimeters behind the sample. In the case of grains of sufficient crystalline perfection, an area beam can be employed to illuminate a sample volume. However, with increasing lattice orientation spread, spot overlap becomes prohibitive, and eventually a line beam must be used that illuminates a single sample layer. A forward modeling reconstruction (FMR) procedure is described for this geometry. The scattering event is modeled explicitly and the orientation of individual sample grid elements is optimized.

At the far-field limit, the sample to detector distance is much larger than the sample dimensions. This provides ample space for sample environment. The strain sensitivity is dramatically improved, but only the center-of-mass grain positions are measured. At intermediate detector distances, several complete diffraction rings are recorded, and grain specific stress tensors can be evaluated. By moving the detector even further back and using a narrow bandwidth x-ray beam, the angular resolution is improved such that peak broadening due to dislocation structure can be analyzed. The latter setting is referred to as high-resolution reciprocal space mapping.

In this paper, both medium and high-resolution reciprocal space far-field

diffraction experiments are demonstrated by an investigation of the plastic deformation of the HCP titanium alloy, Ti-7Al. Investigations on both the grain and subgrain length scales were conducted. Electron microscopy (EM) was performed post-mortem on the same samples and subsets of grains after in situ far-field measurements during uninterrupted tensile deformation. Serial sectioning was applied to obtain bulk information. Finally, we present an application of high-resolution reciprocal space mapping to characterize the evolving dislocation structure in pure copper during tensile deformation. The diffraction signals from individual subgrains are identified and enable a detailed characterization of their behavior.

NEAR-FIELD MICROSTRUCTURE ORIENTATION MAPPING

Figure 1 shows a schematic of the near-field experimental configuration. At the APS, the penetration depth and beam size are well matched and the structure inside millimeter sized samples can be probed. In addition, because of the small source size, special purpose high-energy x-ray optics can focus beams to micron or smaller dimensions. In our near-field microstructure mapping measurements, we focus in one dimension (vertical) but allow the other dimension to remain unfocused. Thus, the sample is illuminated by a planar beam with micron vertical but millimeter horizontal dimensions and measurements are done in transmission. If the beam illuminates a sufficiently small number of grains, diffraction spots generated by individual grains can be isolated and imaged. Because Bragg angles are small at high energies, many diffraction orders can be collected on a small area detector placed millimeters to centimeters behind the sample. For example, at 50 keV, {111} scattering from nickel has a Bragg angle of $\theta = 3.5°$, and a scattering angle, 2θ, of 7°. At 1 cm, this diffraction will have diverged from the incident beam by only 1.2 mm. At 5 mm, a 3×3 mm^2 detector can see (in the configuration of Figure 1) peaks with Miller indices up to {911}. The imaged spots are essentially projections of the shapes of cross-sections of the diffracting grains. The projections are anisotropic: as implied by Figure 1, the x-direction dimension is reproduced essentially 1:1 whereas the grain dimension in the z-direction is compressed in the y-dimension of the detector. This anisotropy depends on both detector coordinates (2θ and η) and can be overcome by obtaining many Bragg spots from each grain with the sample in different orientations.

Our data collection protocol consists of measuring diffraction pattern images as the sample rotates through a small interval in ω, typically one degree. At each detector position, L, 180 contiguous intervals are measured and either two or three L-distances are measured. For cubic crystal structures, random orientations generate roughly 60 Bragg peaks that strike the detector implying that 60 projections are obtained for each grain cross-section in the illuminated plane. All of these projections are used by the FMR procedure described below.

We collect volumetric data by taking 360 (two detector distances) or 540 (three distances) images for each cross-section, translating the sample along the y-axis, and repeating the process. The vertical step size is determined by weighting several factors. In order to determine three-dimensional grain shapes, it should be less than the grain size by at least a factor of ten. To obtain isotropic three-dimensional resolution, it should be approximately equal to the in-plane spatial resolution. Depending on the data acquisition rate, it must be large enough to repeatedly measure a significant volume of material and allow for sample treatments during a typical synchrotron beam time. Compromise values have ranged from four to 20 micron steps between layer measurements. It should be noted that with recent developments, we expect an increase by a factor of about 20 in data acquisition rates relative to the data sets presented here. This will allow for high-resolution studies both in terms of spatial resolution and in the sample treatment steps taken between measurements (annealing, strain, temperature, etc.).

In an attempt to extract as much information from volumetric data sets as possible (noting that the data sets are expensive in terms of experimental facilities, beamtime, and human resources), we use a computationally intensive FMR procedure. The experiment, as described above, is modeled in the computer, the sample plane is meshed with equilateral triangles and, in each triangle, a fundamental zone of crystal orientations is "searched" so as to generate Bragg scattering that optimally overlaps that seen in the measurement. The orientation in each triangle is determined independently from others and is based on matching to the entire data set—about 60 Bragg peaks are assigned to individual triangles. This independence makes parallel computation easy to implement. In preliminary image analysis, CCD images are median filtered to remove hot pixels, a background is subtracted, and peaks are identified. All pixels in a peak that are above some fraction (typically 0.1) of the peak height are set to one while others are set to zero. At this point, the FMR code matches to this binary version of the experimental data. Thus, we are still not extracting as much information as is in the data sets; we are currently implementing intensity matching code. In the case where grains are found to be well-defined entities with little intra-granular orientation variation, a variety of short-cuts can be used to accelerate the reconstruction. As area elements are fitted, a list of resulting distinct orientations can be kept and these can be tested (perhaps with a local Monte Carlo orientation optimization) against the data set; if the match is sufficient, the full orientation space does not need to be tested. Further, once one layer of data has been reconstructed, the adjacent layer(s) can start with neighbor orientation fields and a procedure similar to that just described can be used. In appropriate data sets, one gains at least a factor of ten in reconstruction speed.

The result of the FMR procedure is illustrated in Figure 2a which shows one section of a reconstructed fully recrystallized nickel microstructure. The triangular mesh, consisting of 98,304 triangles with 5.6 μm sides, covers the entire hexagon. In the white space, the reconstruction code found no orientation that generated sufficient match to the data. The circular colored region

corresponds to the 1.1 mm diameter sample cross-section (the notch on the left side resulted when the sample was electric discharge machined). Colors correspond to crystallographic orientation by mapping the three components of the Rodrigues vector to red, green, and blue contributions, respectively. Each colored region contains many triangles–each of which was independently determined to have a similar orientation. In Figure 2a, black lines have been added between any nearest neighbor triangles with orientations that differ by at least 0.1°.[4] These lines mostly outline the grain boundaries. In addition, a few lines appear inside of the grains, but given the 0.1° threshold, their sparse distribution indicates both rather perfect grains and the very good angular resolution of the measurement. This test is quite rigorous since none of the above mentioned shortcuts were used in this reconstruction. Simulations on well ordered, synthetic microstructures indicate an orientation resolution of 0.1°.[5]

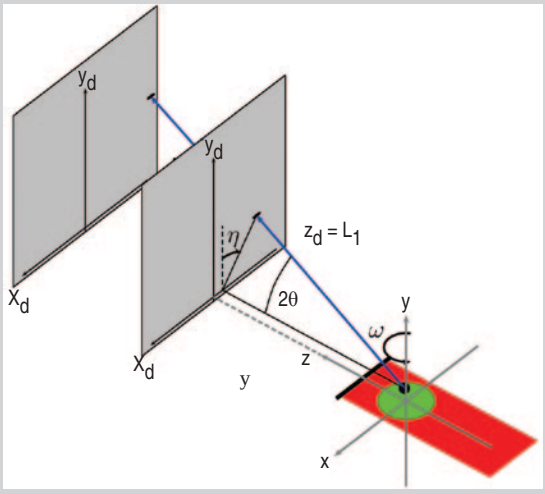

Figure 1. Schematic of the mapping measurement as described in Poulsen,[1] and Suter et al.[3]

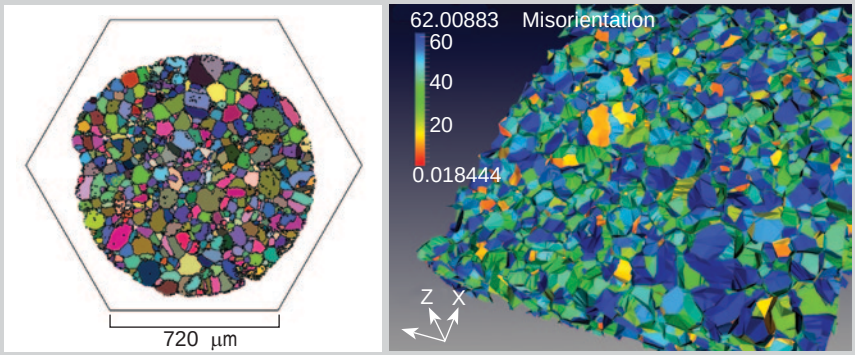

a b

Figure 2. (a) Orientation map of an internal layer of high purity nickel determined using the near-field HEDM method showing several hundred grains of about 40 μm diameter. Black lines indicate orientation discontinuities larger than 0.1°. (b) Stack of 43 layer sections similar to that in (a) meshed into a three-dimensional digital structure. The axis of the cylindrical sample is perpendicular to the shown section. Only boundary mesh elements are shown. Colors are mapped from the misorientation between bounding grains, as is indicated by the scale bar.

Figure 2b shows the result of a volumetric measurement including 43 layers similar to that in (a). We use state-of-the-art meshing code based on the Computational Geometry Algorithms Library,[6] a well tested templated C++ library of general purpose routines. With such meshes plus a feature extraction library (XDM++), we can analyze misorientations (as displayed in the figure), grain sizes, shapes, and connectivity, grain boundary character distributions, as well as others. Given measurements of the same volume before and after processing, differences in structures can be seen. With additional mesh quality improvements, the volume meshes can be inserted into finite element codes and, together with response data, can be used to directly validate or invalidate models and to fix values of unknown parameters in the models.

Figure 3 shows an example of the statistics extraction capabilities of the HEDM mapping measurement. The

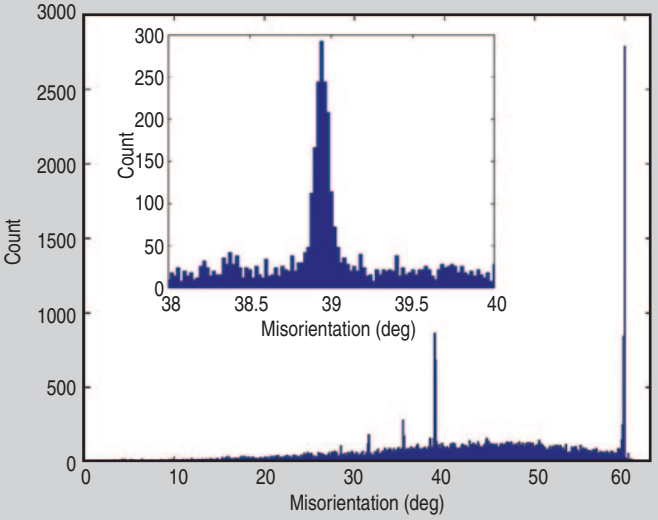

Figure 3. The distribution of misorientation angles between nearest neighbor grains. The angle bin size is 0.1°. The maximum rotation angle required for cubic symmetry is 62.8°. Sharp peaks occur at rotation angles corresponding to coincident site lattice orientation relationships including Σ27a (31.6 °), Σ27b (35.4 °), Σ9 (38.9 °), and Σ3 (60.0 °). Making these Σ-assignments, however, requires specification of the rotation axis in addition to the rotation angles presented here. Each of the sharp peaks has full width at half maximum of 0.1°. The inset shows the peak at 38.9° with a bin size of 0.02°.

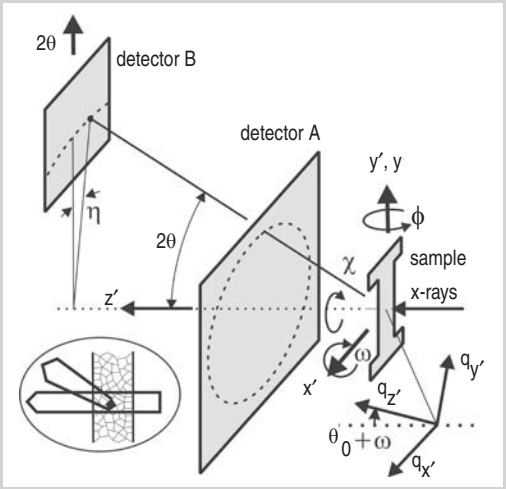

Figure 4. Far-field diffraction setup in the 1-ID-C hutch.[9]

Figure 5. Loading curves of the air-cooled (AC) and ice water quenched (IWQ) Ti-7Al samples. In our latest experiment, the samples were deformed continuously at a nominal strain rate of 10^{-6} s^{-1} while x-ray diffraction patterns were acquired. Reduction of those data is ongoing. Previously, the loading was halted to acquire diffraction data. The approximate macroscopic stress levels where the earlier Ti-7Al diffraction experiments were conducted are depicted as the four red symbols. The data from these diffraction experiments are presented in this paper.

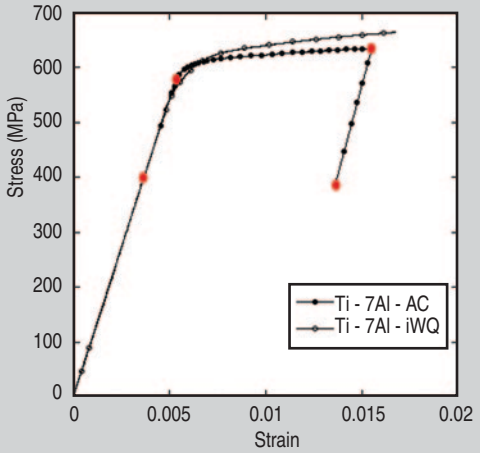

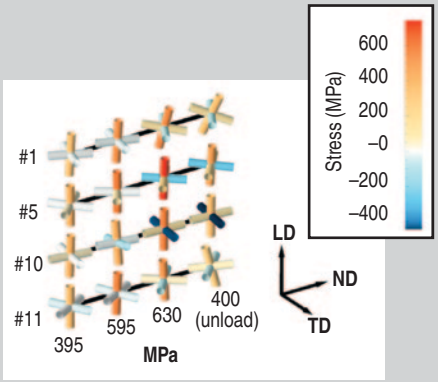

Figure 6. Principal stress triads or "jacks" depicting the orientation and magnitude of the principal stresses experienced by four grains (#1, #5, #10, and #11) within the deforming AC specimen at the indicated macroscopic stress levels (in MPa). These stresses are depicted as the red symbols in Figure 5. The relevant specimen directions, LD (loading direction), TD (transverse direction) and ND (normal directions) are also depicted as is a stress color bar.

Figure 7. Cut through the high-resolution reciprocal space map of a prismatic reflection of the AC reference grain. The abscissa is associated with an azimuthal reciprocal space direction and indicates misorientations, whereas the ordinate is along the radial reciprocal space direction indicating strain. Three domains of distinct orientation are discernable that also display distinct lattice strain distributions. The color bar indicates intensities which are proportional to volume fractions.

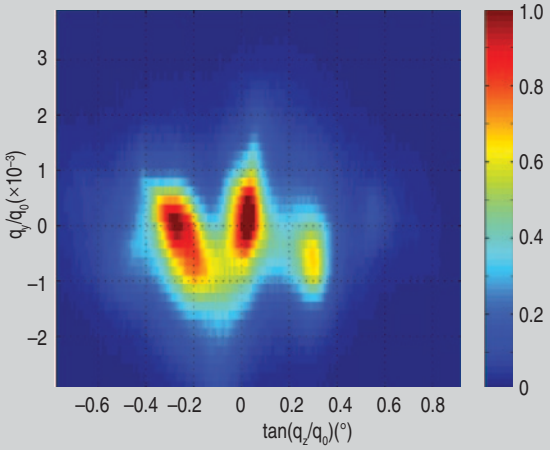

distribution of misorientation angles between nearest neighbor grains shows a smooth distribution (similar to the Mackenzie distribution of randomly oriented cubes) punctuated by sharp peaks at several angles associated with low order coincidence site lattice rotation angles, Σ27a, Σ27b, Σ9, and Σ3. The Σ3 peak corresponds to twin boundaries, a 60° twist about the <111> interface normals. All of the peaks of the misorientation distribution have 0.1° widths which is our orientation resolution—thus, the "special boundary" peaks are surprisingly sharp.[7] The predominance of Σ3 boundaries can also be seen in Figure 2b through the many blue boundaries.

The nickel data set presented here illustrates the ability to obtain detailed orientation maps at several micron resolutions in a well ordered material. We have measured a similar volume of a nickel-bismuth dilute alloy and are in the process of comparing grain boundary character distributions and grain boundary energy distributions.[8] We plan to anneal both of these samples so as to compare the grain growth in well characterized and well ordered materials. In addition, we have measured and reconstructed significantly less well ordered materials and are implement-

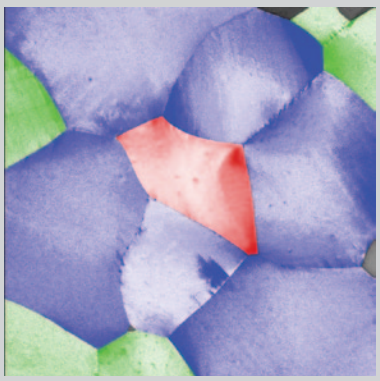

Figure 8. EBSD image containing the AC master grain (red). The image width is 250 μm, the load axis is horizontal, and the color contrast is scaled to a misorientation of 2°. The intragrain contrast indicates that the master grain is subdivided into a small number of misoriented domains. This observation is in agreement with the x-ray high-resolution reciprocal space mapping (see Figure 7). While the in situ x-ray data map lattice strains in orientation space, the EBSD maps orientation in real space and therefore contributes complementary information.

ing measurements of the evolution of microstructures under strain up to the limit of ductile failure. The mapping measurements can also be applied to study a variety of phase transformations and structural domain wall motions such as occur in ferroelectric and other materials.

FAR-FIELD INTER-GRANULAR STRAIN MAPPING AND HIGH-RESOLUTION RECIPROCAL SPACE MAPPING

Tensile Deformation of Ti-7Al

Figure 4 depicts the far-field setup at APS 1-ID-C used for in situ loading/diffraction experiments on Ti-7Al.

The goal of these experiments was to use high-energy x-rays and electron microscopy (EM) to understand the grain scale deformation behavior of this important class of titanium alloy. In particular, we sought to contrast the micromechanical response in two states (named for the cooling rates used after annealing): (i) Air Cooled (AC) material, which is known to contain Short Range Order (SRO) domains and (ii) Ice Water Quenched (IWQ), state without SRO. The different material states give rise to distinct strain hardening. EM has revealed that the AC material develops planar slip bands whereas the IWQ material develops a rather uniform dislocation distribution. We present results here as a means to illustrate the nature of the far-field techniques and their potential for understanding inter- and intragranular micromechanical deformation processes such as deformation partitioning among different grains within a polycrystalline aggregate and dislocation structure evolution. Two different experiments have been performed. First, diffraction measurements were performed at several load steps as indicated in Figure 5 while the deformation was halted (interrupted loading).[9] Recent instrumental advances enabled diffraction measurements in situ during continuous deformation—where loading is not paused. The load curves shown in Figure 5 were recorded during the continuous loading experiment and indicate the relative differences in hardening behavior between the two material states.

As depicted schematically in Figure 4, entire Debye Scherrer rings of data are collected on detector A. Individual reflections are matched with particular grains within the deforming aggregate by indexing software.[10] The samples were rotated about the loading axis by 120° (ϕ) while an image was acquired for each one degree interval. Every crystal within the x-ray beam (300 μm (hor.) ×150 μm (vert.)) diffracts from several sets of lattice planes ($\{hkl\}$s). Each reflection on detector A is uniquely specified with a triplet of angles, (2θ, η, ϕ), which are defined in Figure 4. The diffraction experiment basically involves tracking the diffracted intensities at each load level. The rotation axis is aligned with one grain, which becomes the centering or "master" grain.

About 20 reflections were recorded from each grain and normal strains were evaluated from the 2θ shifts. The grain specific lattice strain tensors were determined by least-square fitting to the normal strain projections. In tracking the diffracted intensity (reflections) from any grain besides the master, we must also account for its distance from the rotation axis. With the single crystal elastic moduli and the lattice strain tensor from each grain, we are able to calculate the full stress tensor experienced by each grain within the aggregate. We also obtain the vector from the centroid of the master grain to the centroid of all other grains. Figure 6 depicts the stress state of four crystals within the Ti-7Al AC aggregate at four macroscopic stress levels (red symbols in Figure 5). The first two stress levels are within the elastic regime and all crystal stress states are close to uniaxial tension. Upon yielding, the rotation of each stress-jack is consistent with a facetted single crystal yield surface associated with restricted slip.[11]

A comparison of the crystal stress states at the first and last macroscopic stress levels (395 MPa and 400 MPa) provides a demonstration of plasticity-induced changes in the stresses experienced by individual crystals. Because of the importance of the grain scale stress state for processes such as microcrack initiation and microplasticity, the variations of stress state seen in Figure 6 as well as their deviation from the uniaxial macroscopic condition are the most important observations from these experiments. As the sophistication of crystal-scale models improves, HEDM data will prove invaluable for both instantiation of identical virtual polycrystals and for validation of stress state predictions.

Due to the large distance from detector B to the deforming sample and the narrow bandwidth of the incident x-ray beam, data collected there are high-resolution two-dimensional cuts through the reciprocal space intensity distribution of the selected reflection. Details of the high-resolution space mapping technique are given by Jakobsen et al.[12] Three-dimensional reciprocal space maps are obtained by transforming successive images recorded on detector B while rotating the sample in small intervals around the ω-axis. A perfect lattice produces a reciprocal space map with sharp peaks associated with each lattice plane, $\{hkl\}$. As the grain deforms and the lattice strains, the peaks shift and broaden. Figure 7 shows a cut through the reciprocal space intensity distribution for a prismatic reflection of the AC master grain from the continuous deformation experiment. The data were recorded after the continuous loading was terminated and the load was reduced to prevent creep. Before deformation, all intensity was concentrated in a few pixels, i.e. instrumental broadening can be neglected. Three distinct domains, which are associated with changes in lattice orientation, are resolved along the azimuthal direction (abscissa). It is obvious that the domains have distinct strain values. Thus, a determination of dislocation density from the width of radial distributions has to be domain specific as the inter-domain strains broaden the grain integrated radial distribution. During recent experiments, high-resolution reciprocal space maps were recorded for 12 reflections for the AC and IWQ master grains. These data sets should enable the reconstruction of the grain specific orientation distribution and the lattice strain distribution[13] for model comparison. It should be noted that the reciprocal space maps do not provide any spatial information. Therefore, post-mortem EM can provide largely complemen-

tary information if the samples are serial sectioned after the experiment. The location of the master grains were carefully documented during recent experiments and serial sectioning experiments with electron backscatter diffraction (EBSD) were performed post-mortem. An EBSD imaged section through the AC master grain is shown in Figure 8. It is seen that the grain splits into a small number of misoriented domains, in agreement to the described x-ray reciprocal space mapping.

Furthermore, foils were extracted from within the AC master grain and investigated by TEM. Such high real space resolution data cannot be obtained by the described x-ray techniques and enable the characterization of individual dislocations and their distribution. Models have also been developed to extract dislocation character and density from the radial peak profiles of high reciprocal space resolution x-ray data (e.g. by Wilkens[14], Ungár[15]). However, the x-ray reciprocal space maps described above integrate over the volume of individual grains and spatial heterogeneities must be taken into account for quantitative peak shape analysis. The TEM observations provide a benchmark for the ongoing x-ray peak profile analysis.

We now present an example of combining HEDM lattice strain data with highly resolved finite element method (FEM) simulations of the Ti-7Al. Figure 9 presents modeling results for the stress state relative to the single crystal yield surface as well as slip system activity.

Dislocation Structure Evolution in Copper under Tensile Deformation

Plastic deformation of metals such as copper is accomplished by motion of dislocations. These line defects are stored in the material as self-organized, ordered dislocation structures. In deformation-induced microstructures, dislocation-rich walls (dislocation boundaries) separate dislocation-depleted regions of slightly different orientations. Both microstructural constituents can be distinguished using high-angular resolution x-ray diffraction by their different signature on x-ray reflections. This situation is different from that for the described high resolution Ti-7Al measurements (Figure 7) where no individual subgrains are resolved. Reciprocal space maps of individual x-ray reflections obtained with high angular resolution (recorded on detector B in Figure 4) reveal a small number of sharp, high-intensity peaks on top of a spread-out, smoothly varying intensity distribution[12] (Figure 10). The latter cloud contribution arises from the disordered dislocation walls, whereas the individual sharp peaks are the signatures of nearly perfect subgrains. By analysing the behavior of the high-intensity peaks during deformation, properties of the related subgrains can be investigated and their evolution monitored in situ (Figure 11). This is illustrated for copper deformed in tension.[12] A particular grain with desired orientation is selected in the bulk of a polycrystalline specimen. Reciprocal space maps of a {400} reflection close to the tensile axis are recorded. By reciprocal space mapping the evolution of the deformation-induced microstructure can be followed during different loading regimes: tensile straining, stress relaxation[17] (Figure 12), unloading, or strain path changes.[18]

SUMMARY AND CONCLUSIONS

This paper provides an overview of the High-Energy Diffraction Microscopy (HEDM) suite of experiments under continued development at the Advanced Photon Source (APS) beamline 1-ID. These experiments are designed to quantify grain scale structure and mechanical response within deforming polycrystalline alloys. The data from HEDM experiments are providing important information regarding deformation and damage evolution at the most important size scales. The microstructural characterization data from near-field HEDM experiments are comparable to the results from the current generation of serial sectioning/EBSD experiments, which provide three-dimensional orientation reconstructions of polycrystalline aggregates. The important distinction is the non-destructive nature of the HEDM experiments.

Grain boundary topology can be mapped in the near-field geometry whereas strain and stress states of individual grains are mapped in the far-field setting during in situ loading conditions. The lattice strain tensors of individual grains within a deforming polycrystal can be measured with resolution of the order of 10^{-4}. The relatively small number of grains that are possible to interrogate in a typical HEDM lattice strain experiment has been a limitation in the past—making it difficult to interpret the applicability of the findings. Recent data sets cover statistically representative numbers of grains (hundreds to thousands).

Evolving dislocation structure is investigated by in situ high-resolution reciprocal space mapping and can be augmented by post-mortem EM. These multiple length scale data open a unique opportunity to validate and develop micromechanical models. There exists enormous potential for drastically improving our understanding of grain scale mechanical processes by using these unique experimental results together with modeling formulations. Large potential lies in software advances reconstructing strain distributions in real and orientation space. Significant experimental progress is possible by technological evolution that is currently occurring in the areas of x-ray production and detection. At present, a dedicated experimental station is being designed at the 1-ID beamline that will enable the simultaneous acquisition of near- and far-field data. This will make it possible to replicate the microstructural details within the polycrystalline aggregate and the resulting unique stress states experienced by each of the deforming crystals. Furthermore, a new thermo-mechanical sample environment stage is being developed capable of high fidelity cyclic loading. Dedicated x-ray optics will also provide sub-micron sized beams aiming at a "zoom-in" micro-diffraction option once interesting features are identified by the fast "tomographic" scan modes.

ACKNOWLEDGEMENTS

Work at CMU was supported by the MRSEC program of the National Science Foundation under award number DMR-0520425 and the NSF Metals program under award number DMR-0805100; NSF TeraGrid resources were provided by the Pittsburgh Su-

percomputing Center. Cornell gratefully acknowledges the Office of Naval Research, Julie Christodoulou, Grant Officer for support of this work as part of the D 3-D Program, contract number N00014-05-1-0505. Work at Risø DTU was supported by the Danish National Research Foundation through funding of the Center of Fundamental Research: Metal Structures in Four Dimensions and the Danish Natural Science Research Council. Use of the

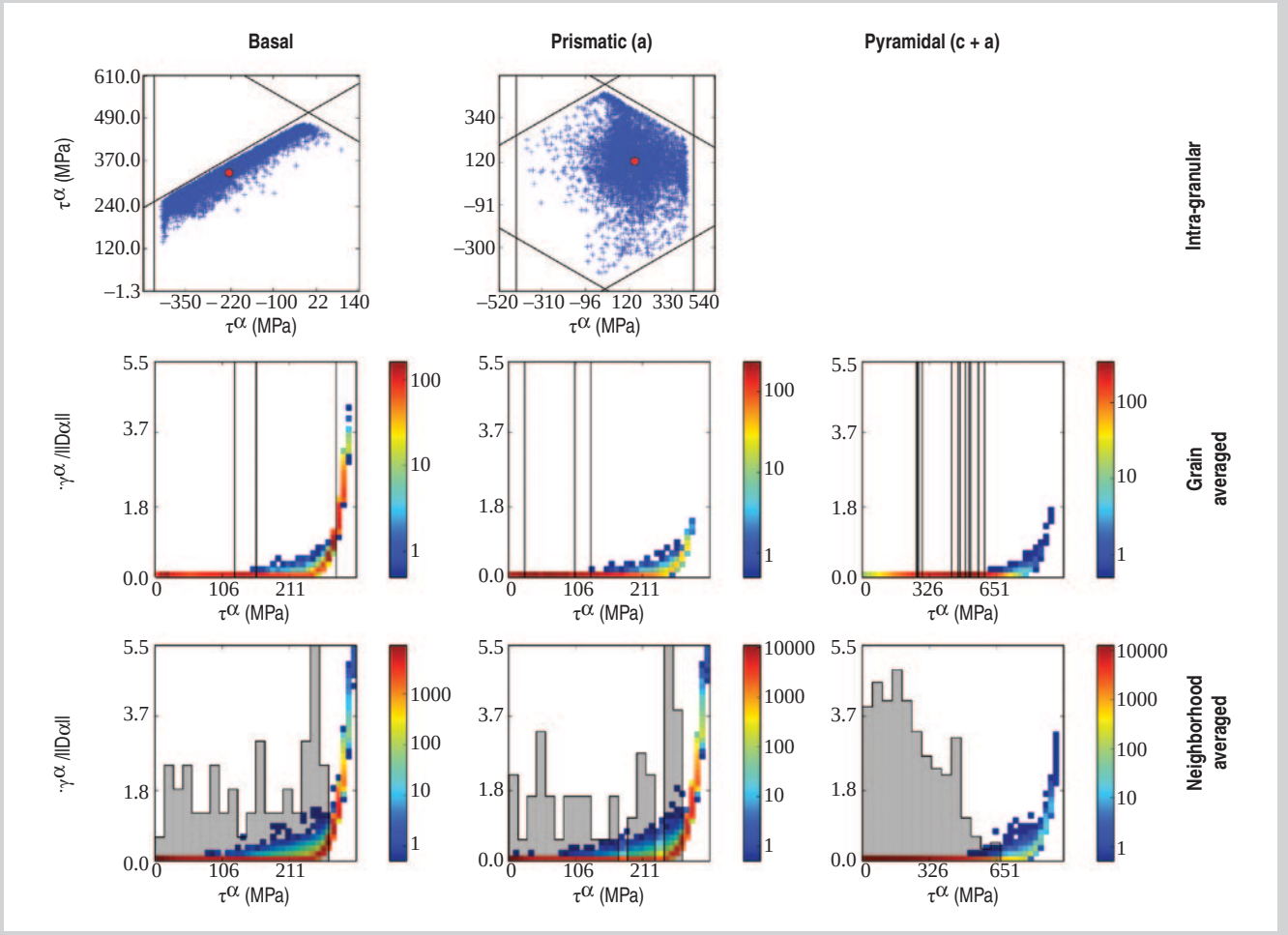

Figure 9: FEM simulation. The underlying mesh is based on the experimentally measured centroidal grain coordinates (details are given in Bernier et al.[16]). Each complete grain is composed of several thousand finite elements; this level of discretization facilitates a significant amount of intra-granular heterogeneity to develop. The elastic and plastic material parameters were adjusted to match the stress-strain data for the alloy, and the aggregate was subsequently deformed in uniaxial tension out to ~2% plastic strain as in the experiment.

Top row: sections of deviatoric stress space spanned by the basal $\langle 2\bar{1}\bar{1}0\rangle\{0001\}$ and prismatic $\langle \bar{2}110\rangle\{01\bar{1}0\}$ slip systems; each defines a two-dimensional surface in the full five-dimensional space. The black lines represent the traces of the reference CRSS values for each slip system, $\tau : P^a - g^a$, where τ is the Cauchy stress, P^a is the deviator of the Schmid tensor for the α^{th} slip system, and g^a are the corresponding reference CRSS values. These figures approximate yield surface sections at fixed state; edges correspond to facets, and vertices correspond to edges. The pyramidal slip systems do not describe a simple two-dimensional subspace, nor are they on average active in the incipient plasticity regime examined, and therefore are not shown. Blue points are the projections of the stresses from each element discretizing the grain into the respective stress subspace. Red points are the projections of the stress obtained via the volume-averaged strain tensor over the grain, and thus approximate the type of stress available from the far-field HEDM experiment. Points near the envelope denote "active" slip systems under the power-law slip kinetics, and the spread is indicative of the intra-granular deformation heterogeneity. That the red points lie near the center of these clouds is not at all surprising; it does illustrate, however, that the average stress lies at a point that is consistent with the bulk slip system activity. For this grain, one basal slip system is active.

Middle row: Two-dimensional histograms of slip activity over the grain for each denoted slip system. The color represents counts on a log scale plotted against normalized shearing rate, $\dot{\gamma}^\alpha / \|D_\alpha\|$ where D_a is the applied rate-of-deformation tensor, and resolved shear stress, $\tau^a - t : P^a$, for each slip system. The black lines along the τ^a axes represent the values calculated from the grain volume-averaged stress for each individual slip system. The shape of the histograms for active slip systems reflect the underlying power law kinetics and display a clear "knee" with high count densities around the CRSS values. The histograms for largely inactive slip systems generally lack the knee and have peak counts along the tail at stress magnitudes below the corresponding CRSS value.

Bottom row: Inter-granular stress data over the grain neighborhood as composite histograms. The colored two-dimensional histograms represent the aggregate of the grain-level histograms (as above) over the neighborhood. The superimposed grey histograms represent the τ^a values calculated from the grain-averaged stresses over each slip system. Note that slip systems that are active over the neighborhood display $\dot{\gamma}^\alpha / \|D_a\| - \tau^a$ histograms consistent with the single-grain counterparts: a clear knee with a high counting density at the CRSS value. What is interesting, however, is that the purely inter-granular histograms (i.e., the grey bars) also display a peak at a stress magnitude that coincides quite closely with the CRSS value. Meanwhile the histograms for the inactive pyramidal slip systems display no such peak at the tail. This important result indicates that despite the intra-granular heterogeneity, the statistics over the volume-averaged stresses from each grain in the neighborhood are sufficient for capturing the underlying CRSS values.

Advanced Photon Source was supported by the U.S. Department of Energy, Office of Science, Office of Basic Energy Sciences, under Contract No. DE-AC02-06CH11357. Part of this work was performed under the auspices of the U.S. Department of Energy by Lawrence Livermore National Laboratory under Contract DE-AC52-07NA27344, with funding supplied by Laboratory Directed Research and Development grant 10-ERD-053.

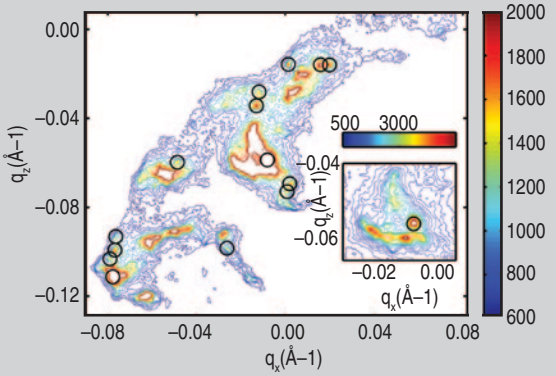

Figure 10: Azimuthal projection of the reciprocal space map of a {400} reflection from a single grain (oriented such that the [100] direction was near the loading direction) in a copper specimen after 2% tensile deformation.[12] Sharp, high-intensity peaks are superimposed on a smoothly varying cloud. The insert is an enlargement of the peak intensity region showing that it in fact consists of several individual peaks as well. The 14 selected peaks that were further analyzed in Figure 11 are marked by circles.

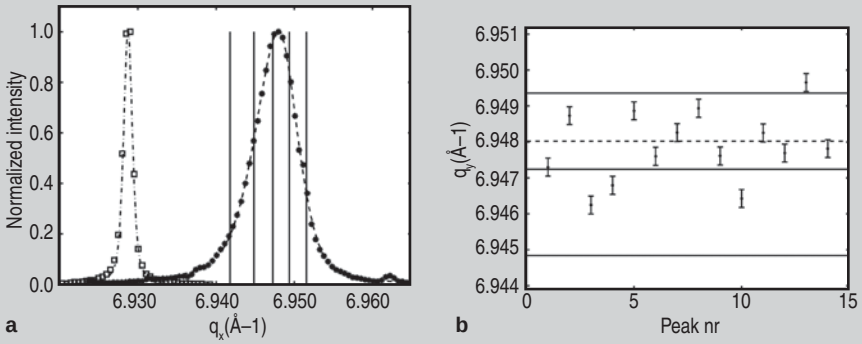

Figure 11: (a) Radial intensity profile (indicating strain) of a {400} reflection from a single grain in a copper specimen after 2% tensile deformation. The intensity profile from LaB_6 powder is included for comparison (open squares). The vertical lines indicate the 10%, 25%, 50%, 75%, and 90% quantiles. (b) The radial positions of 14 selected peaks compared to the radial position of maximum intensity and the 25%, 50% and 75% quantiles of the radial profile for the entire grain. The peaks occur at quite different radial positions and hence the associated subgrains experience quite different elastic strains. Obviously, the peaks are not spread evenly around the median (corresponding closely to the average intensity), but gather around the position of maximum intensity indicating an overall back strain of the subgrains compared to the average elastic strain of the grain.[12]

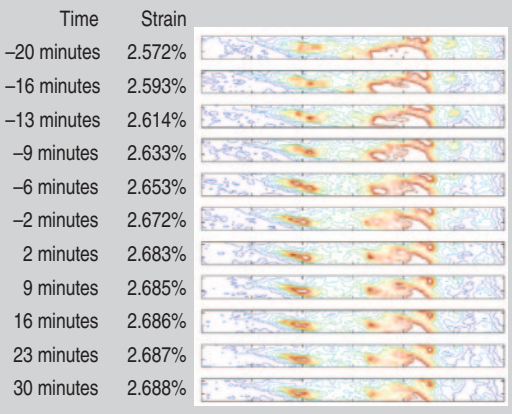

Figure 12. Azimuthal projections of reciprocal space maps of a {400} reflection from a single grain during tensile loading and stress relaxation.[17] The time is specified with respect to the instant of stopping the tension motor. As long as deformation proceeds significant changes in the subgrain structure are observable from the reciprocal space maps. Temporary formation of new subgrains and disappearance of others can be recognized. During the holding stage, there is no evidence of any microstructural change on the subgrain level, but the width of the radial profile decreases indicating a decrease in the variation of elastic strains within the grain.

References

1. H.F. Poulsen, *Three-Dimensional X-ray Diffraction Microscopy, Springer Tracts in Modern Physics, Vol. 205,* ed. G. Hohler (Berlin: Springer, 2004).
2. S.D. Shastri, J. Almer, C. Ribbing, and B.J. Cederstrom, *Synchrotron Rad.,* 14 (2007), pp. 204–211.
3. R.M. Suter, D. Hennessy, C. Xiao, and U. Lienert, *Rev. Sci. Instrum.,* 77 (2006), p. 123905.
4. C.M. Hefferan, S.F. Li, J. Lind, U. Lienert, A.D. Rollett, P. Wynblatt, and R.M. Suter, *Computers, Materials and Continua,* 14 (2009), pp. 209–219.
5. C.M. Hefferan, S.F. Li, J. Lind, and R.M. Suter, *J. Powder Diffraction,* 25 (2010), pp. 132–137.
6. CGAL, Computational Geometry Algorithms Library, *http://www.cgal.org.*
7. D.G. Brandon, *Acta Mater.,* 14 (1966), pp. 1479–1484.
8. J. Li, S.J. Dillon, and G.S. Rohrer, *Acta Mater.,* **57** (2009), pp. 4304–4311.
9. U. Lienert, M.C. Brandes, J.V. Bernier, J. Weiss, S.D. Shastri, M.J. Mills, and M.P. Miller, *Mater. Sci. Eng. A,* 524 (2009), pp. 46–54.
10. E.M. Lauridsen, S. Schmidt, R.M. Suter, and H.F. Poulsen, *J. Appl. Crystallogr.,* 34 (2001), p. 744.
11. U.F. Kocks, *Metall. Trans.,* 1 (1970), p. 1121.
12. B. Jakobsen, H.F. Poulsen, U. Lienert, and W. Pantleon, *Acta Mater.,* 55 (2007), pp. 3421–3430.
13. J.V. Bernier and M.P. Miller, *J. Appl. Crystallogr.,* 39 (2006), pp. 358–368.
14. M. Wilkens, *phys. stat. sol. (a),* 2 (1970), p. 359.
15. T. Ungár, *Mater. Sci. Eng. A,* 309-310 (2001), pp. 14–22.
16. J.V. Bernier, N.R. Barton, M.C. Brandes, U. Lienert, M.P. Miller, and M.J. Mills, *Proc. 31st Risø International Symposium on Materials Science,* ed. N. Hansen et al. (Risø, Denmark: Risø National Laboratory for Sustainable Energy, Technical University of Denmark, 2010), pp. 251-259.
17. B. Jakobsen, H.F. Poulsen, U. Lienert, J. Bernier, C. Gundlach, and W. Pantleon, *phys. stat. sol. (a),* 206 (2009), pp. 21–30.
18. W. Pantleon, C. Wejdemann, B. Jakobsen, U. Lienert, and H.F. Poulsen, *Mater. Sci. Eng. A,* 524 (2009), pp. 55–63.

U. Lienert, staff scientist, is with Argonne National Laboratory, 9700 S. Cass Ave., Lemont, IL 60439, USA, (630) 252-0120, e-mail lienert@aps.anl.gov; S.F. Li, C.M. Hefferan, J. Lind, and R.M. Suter are with Carnegie Mellon University, Pittsburgh, PA 15213, USA; J.V. Bernier and N.R. Barton are with Lawrence Livermore National Laboratory, Livermore, CA 94551, USA; M.C. Brandes, research scientist in the Department of Materials Science, and M.J. Mills are with Ohio State University, 477 Watts Hall, Columbus, OH 43210, USA; M.P. Miller is with Cornell University, 194 Rhodes Hall, Ithaca, NY 14853, USA; B. Jakobsen is with Roskilde University, Universitetsvej 1, 4000 Roskilde, DK; B. Jakobsen and W. Pantleon, senior researcher, are with Risø DTU, Frederiksborgvej 399, 4000 Roskilde, DK.